International Journal on Magnetic Particle Imaging
Vol 4, No 1, Article ID 1810001, 7 Pages

Infinite Science Publishing

Research Article

First Measurement and SNR Results of a 3D Magnetic Particle Spectrometer

Xin Chen[a,*] · Matthias Graeser[a] · André Behrends[a] · Anselm von Gladiss[a] · Thorsten M. Buzug[a]

[a]Institute of Medical Engineering, University of Lübeck, Germany
*Corresponding author, email: {chen, buzug}@imt.uni-luebeck.de

Received 21 August 2017; Accepted 24 July 2018; Published online 17 October 2018

Abstract

A Magnetic Particle Spectrometer (MPS) can emulate the magnetic field inside an MPI imaging device and record the response of the superparamagnetic iron oxide (SPIO) nanoparticles. Therefore, an MPS can be used to measure the characteristics of SPIO nanoparticles and estimate their performance in an imaging device. A one-dimensional and a two-dimensional MPS were introduced before and showed good usability. A three-dimensional transmit coil setup was introduced lately, and its corresponding signal chains have been partially described. This paper will present the first three-dimensional MPS and its first measurement and signal-to-noise ratio (SNR) results.

I. Introduction

In 2005 Bernhard Gleich and Jürgen Weizenecker introduced MPI as a novel imaging technology. It provides sub-millimeter spatial resolution and fast acquisition time for medical imaging [1, 2]. Three-dimensional real-time in-vivo experiments demonstrated a beating mouse heart with high temporal and spatial resolution, using a clinically approved tracer with tolerable concentration [3, 4]. MPI takes advantage of the non-linear magnetization characteristic of SPIO nanoparticles. If an oscillating magnetic field is applied, the nanoparticles exhibit a time-varying magnetization, which will induce a signal in the receive coils. In order to localize the nanoparticles, a static gradient magnetic field is superimposed to limit the response area to a small region nearby the field free point (FFP) or field free line (FFL) depending on the encoding scheme. Namely, all the nanoparticles outside this region are saturated and the response signal drops significantly with distance to the FFP or FFL. In an MPS, the static gradient field is emulated by a homogeneous offset field [5], so the response of the nanoparticles at an arbitrary spatial position in the corresponding MPI scanner can be measured [6].

The performance of the nanoparticles in tracer fluid can be influenced by the diameter of the particle size, crystallinity, surface coating and multiple other particle properties, as well as the concentration of the fluid, the viscosity of the medium, the excitation frequency and the strength of excitation magnetic fields. To investigate these influences, the MPS is used as a tool to estimate the behavior of the nanoparticles and determine their usability for MPI [7–9].

In MPI, the receive signal can be used to reconstruct an image describing the spatial distribution of the nanoparticles. Image reconstruction can be done by solving an inverse problem using a system matrix, which describes the relation between the spatial positions of SPIO nanoparticles and the measured signals [10]. A common method to acquire a system matrix, known as the measurement-based method, is to measure the system response of a known nanoparticle sample (calibration sample) at multiple spatial positions inside the field of view (FOV) [1, 3, 11]. Usually, the calibration sample is shifted by a robot, which is very time-consuming. Besides, due to the quantity of nanoparticles consisting in

the calibration sample at a desired concentration, there is a trade-off involved in choosing the optimum size of the calibration sample. According to [12], if the calibration sample is chosen too big or too small, either the SNR of the measured system matrix or the spatial discretization will influence the resolution of the reconstructed images. Another method to acquire a system matrix is a mathematical approach, called model-based method [13, 14], which simulates the system matrix with maximum SNR and arbitrary discretization. However, it is limited due to the absence of a realistic particle model. Therefore, a hybrid approach was introduced. The response of the nanoparticles is measured in an MPS, where the field geometry of an MPI scanner is emulated. As the calibration sample does not need to be moved mechanically by a robot inside an MPS, the acquisition time of a hybrid system matrix is much faster than using the measurement-based method [5, 6, 15, 16].

II. Motivation

Compared to the measurement-based method, the hybrid approach is expected to significantly reduce the acquisition time and achieve better spatial resolution. In addition, the advantages typically related to the measurement-based method are still maintained. Namely, the hybrid system matrix contains information about the field geometry and the real behavior of the nanoparticles, which currently cannot be included in the model-based method with sufficient accuracy. One-dimensional [7, 17] and two-dimensional [18, 19] MPSs have been implemented and used in several experiments. However, only 2D hybrid system matrices can be recorded so far. Since 3D MPI imaging systems use three-dimensional sequences to excite the nanoparticles, a 3D MPS is indispensable to measure the response of the nanoparticles and record 3D hybrid system matrices.

A coil setup for the three-dimensional MPS has been introduced in [20]. It features pairs of quasi-rectangular coils, which provide a low power consumption and more efficient usage of space. The corresponding signal chains have been partially implemented [21], including the receive coils, the impedance matching between the power amplifier and the transmit coils, as well as the decoupling between three transmit channels. This paper will describe the design of the quasi-rectangular coil setup in detail, as well as the implemented signal chains. Moreover, the measurement and SNR results of the three-dimensional MPS will be demonstrated the first time. In order to match the field strength of a commercially available MPI scanner (MPI25/20FF, Bruker BioSpin MRI GmbH, Ettlingen, Germany), the measurements are performed with a field strength of 12 mT/μ_0 in each spatial direction. However, the presented coil setup is designed to handle a maximum field strength of 20 mT/μ_0.

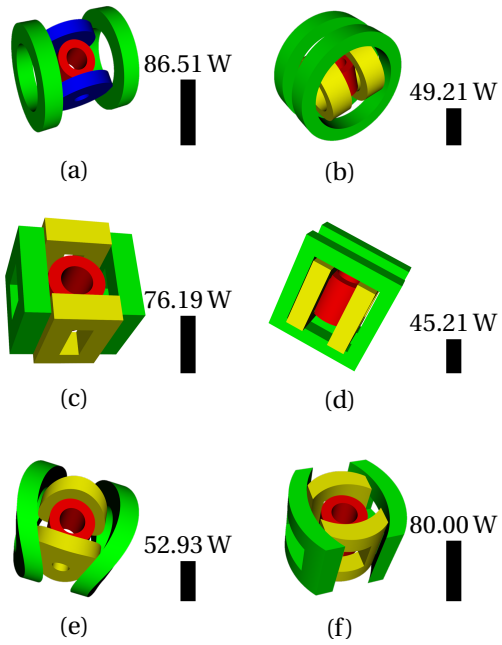

Figure 1: Different coil setups and their simulated powerlosses for a magnetic field of 20 mT/μ_0. (a): flat circular; (b): crossed flat circular; (c): flat rectangular; (d): crossed flat rectangular; (e): curved circular; (f): curved rectangular.

III. Material and Methods

III.I. Coil Setup

Transmit Coils

The central transmit coil is a solenoid coil, which has an outer diameter of 31 mm, an inner diameter of 17.4 mm and a length of 30 mm. It generates a magnetic field in direction X, which is referred to as transmit coil X. The transmit coils in perpendicular directions of X, namely in Y and Z directions, are Helmholtz-like pairs of coils and are referred to as transmit coil Y and Z, respectively. A litz wire manufactured by Elektrisola® is chosen to carry the high frequency current, which has 1000×0.05 mm strands, 2 mm diameter and 9.2 mΩ/m resistance.

Different coil setups have been compared in the simulation concerning the power consumption necessary to produce a magnetic field of 20 mT/μ_0, the corresponding powerlosses are shown in Figure 1. The crossed flat rectangular coil setup has the lowest powerloss of 45.21 W, comparing to the flat circular coil setup with a powerloss of 86.51 W, it is only 52.3 % of the latter. It can be further improved by decreasing the distance between the coils in transmit coil Y, as well as in transmit coil Z. In the simulation, when the distance is decreased to 0, the corresponding coil setup has a powerloss of 29.67 W. However, it is a not practical design, because the central sample chamber would not be possible to access. There-

10.18416/ijmpi.2018.1810001

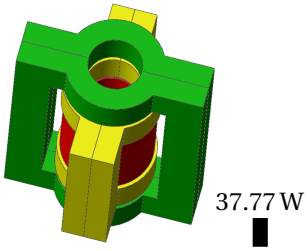

Figure 2: 3D model of the quasi-rectangular coil setup.

fore, a quasi-rectangular coil setup as shown in Figure 2 is designed to ensure that the central sample chamber can be easily accessed. The simulated powerloss of the quasi-rectangular coil setup is 37.77 W, which is 43.7 % of the flat circular coil setup.

Because of the relatively low powerloss, the quasi-rectangular coil setup is chosen to be used in the 3D MPS. Since the response of the nanoparticles can be measured without moving them and homogeneous particle distribution in the sample is assumed, the field homogeneity is not a restrictive factor here. The designed size of the quasi-rectangular transmit coil Y is 55 mm × 57 mm, of the quasi-rectangular transmit coil Z is 63 mm × 83 mm, and the arc has a 8.7 mm radius. For generating the desired field, the applied currents are $11.0\,A_p$, $18.4\,A_p$ and $22.4\,A_p$ for the transmit coil X, Y and Z, respectively. The calculated total powerloss is 49.88 W, which is about 32 % more than the result from the simulation. The increase of powerloss is a result of the manufacturing imperfections of coils and the DC resistance used in the simulation. To implement a Lissajous trajectory, superposed orthogonal signals which feature a common base frequency are necessary. The frequencies chosen in the current system are:

- $f_x = 2.5\,\text{MHz}/102 \approx 24.51\,\text{kHz}$
- $f_y = 2.5\,\text{MHz}/96 \approx 26.04\,\text{kHz}$
- $f_z = 2.5\,\text{MHz}/99 \approx 25.25\,\text{kHz}$

These frequencies are identical to that used in the MPI scanner (MPI25/20FF, Bruker BioSpin MRI GmbH, Ettlingen, Germany). The fabricated quasi-rectangular coil setup is shown in Figure 3. To ensure the perpendicular alignment of the coils, a coil frame is designed to fix their relative positions to each other (see Figure 3).

Receive Coils

In order to achieve high sensitivity, the receive coils are placed as close to the sample as possible. The receive coil in the X direction is a solenoid-like coil. Because the tip part of the sample vial is of conic shape, the middle part of the coil is further modified to form a "sand-clock" shape. The receive coils in Y and Z directions are rectangular saddle coils, which can be easily constructed on cylindrical shells to form a very compact setup.

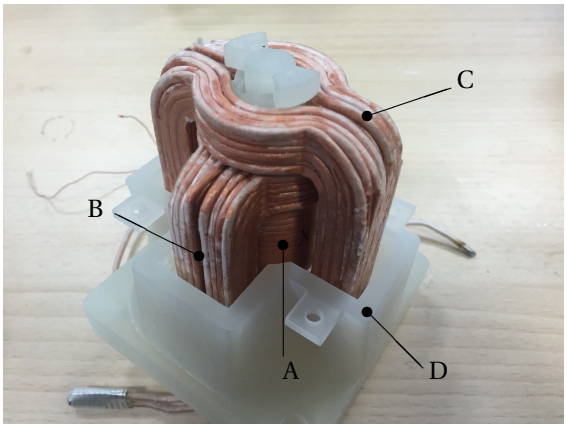

Figure 3: Picture of transmit coils. A: transmit coil X; B: transmit coil Y; C: transmit coil Z; D: coil frame.

In X direction, the sand-clock coil has the biggest radius of 5.4 mm and a length of 18 mm. In Y direction, the side length of the coil is 18 mm × 22 mm, the curvature is 7 mm. In Z direction, the side length of the coil is 21.6 mm × 27 mm, the curvature is 8.6 mm. The assembled receive coil setup can be seen in Figure 4.

III.II. Signal Chains

In Figure 5, a diagram of the signal chains is given. First, the signals are generated in a PC and converted to analog signals by a digital-to-analog converter (DAC). Subsequently, the generated signals will pass the following stages to the transmit coils.

Power Amplifier

The power in each channel is used to supply two identical coil setups, while one is used for generating excitation signals and the other is used in the cancellation unit, which will be introduced later. The power amplifier needs to supply 8.2 W, 52.5 W and 108.8 W to channel X, Y, and Z, respectively. With respect to the measured total powerloss of the transmit coil setup shown above, the increase of powerloss is 69.9 %. It is caused by the shielding and the filters in the system, as well as the direct coupling effect between coils in different channels and the proximity effect.

Due to the imperfection of the amplifier, harmonics of the excitation signals are introduced, which will superimpose the nanoparticles' response due to inductive coupling. The power amplifier modules used here are from Holton Precision Audio, type HPA-NXV200L, which features low harmonic distortion. During the experiments, the amplitude of the input signals has been determined by measuring the currents in the transmit coils.

10.18416/ijmpi.2018.1810001

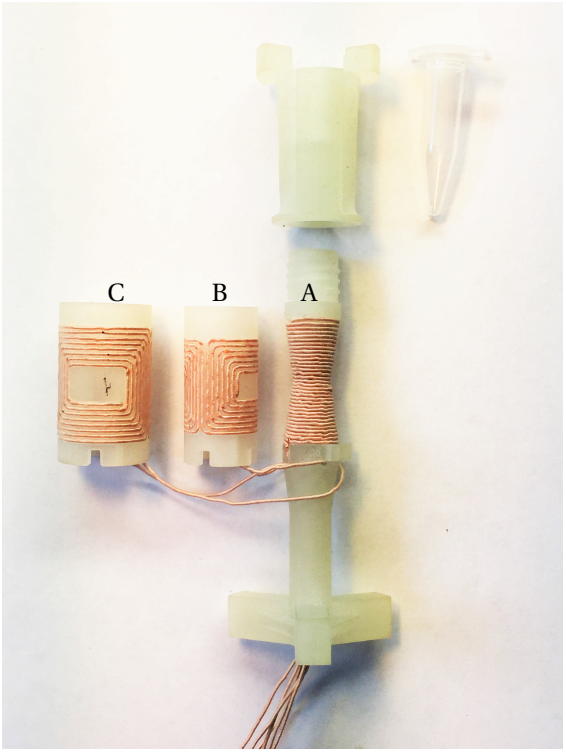

Figure 4: Picture of receive coils. A: sand-clock coil in X direction; B: rectangular saddle coil in Y direction; C: rectangular saddle coil in Z direction.

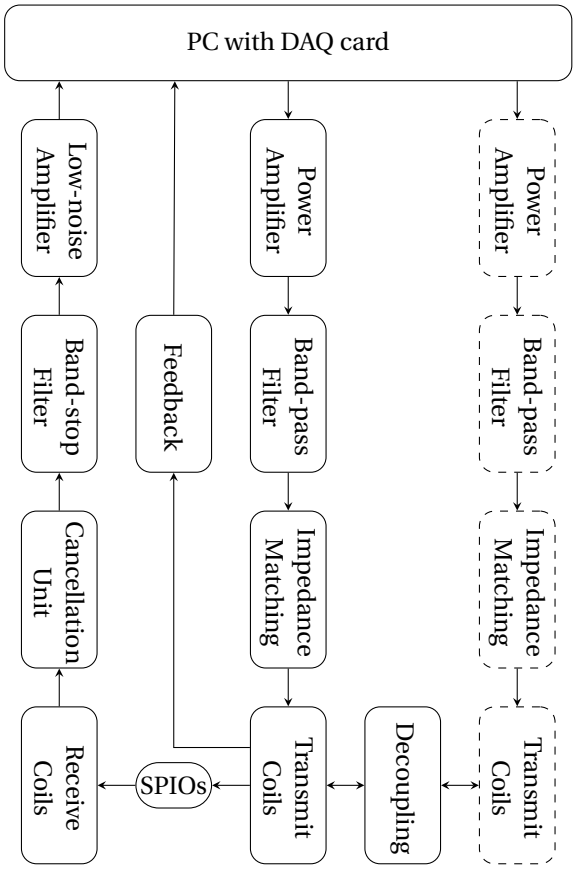

Figure 5: Diagram of MPS signal chains. The signals generated at the DAQ card are amplified and band-pass filtered. The impedance of the transmit coils is matched to the power amplifier by a capacitive matching network. A feedback is used to control the generated fields. The decoupling applied between transmit coils in each channel decreases the influence of coupling. The induced nanoparticles' signals are then band-stop filtered, amplified and digitized. In the diagram, the signal chain of one channel is fully shown, the items in dotted squares represent parts of the other channels.

Band-pass Filter

A band-pass filter (BPF) is used to purify the amplified signals, because of the remaining harmonics of the power amplifier. Here, a third-order LC band-pass filter is built for every channel to suppress the harmonics of the excitation signals.

Impedance Matching

The power amplifiers from Holton Precision Audio can transfer 150 W to a load with 8 Ω, which is sufficient for every channel. Therefore, the transmit coils are matched to 8 Ω by a capacitive network.

Afterwards, the signals are applied to the transmit coils to generate the magnetic fields. Meanwhile, due to the high currents, the consumed power makes cooling essential for continuous measurement. Here, blowers with 36.7 CFM as well as specially designed coil frames are used, which can stabilize the temperature of the coils at 54 °C for continuous measurement at a magnetic field strength of 20 mT/μ_0.

Decoupling

Because the transmit coils are placed very close to each other and it is impossible to ensure perfect perpendicularity, the coupling effect between them cannot be neglected. Hence, a capacitive decoupling between each transmit channel is made to reduce the interference.

Feedback

The voltage across the transmit coils is measured by a resistive feedback loop, which ensures the defined magnetic field is generated.

The nanoparticles placed in the center of the transmit coils are excited and exhibit a time-varying magnetization, which induces a signal in the receive coils. The induced signal will undergo the following stages back to the PC.

10.18416/ijmpi.2018.1810001

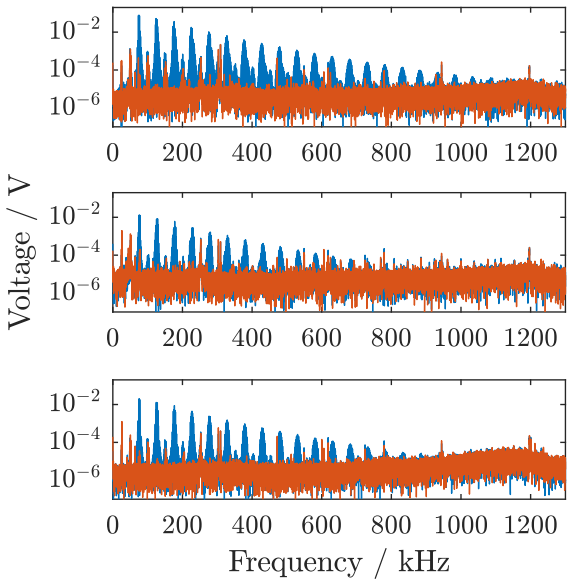

Figure 6: Measured results of three channels without averaging. The results of the receive signals with background subtraction are shown in blue, the remaining backgrounds are shown in red. Upper: channel X; Middle: channel Y; Lower: channel Z.

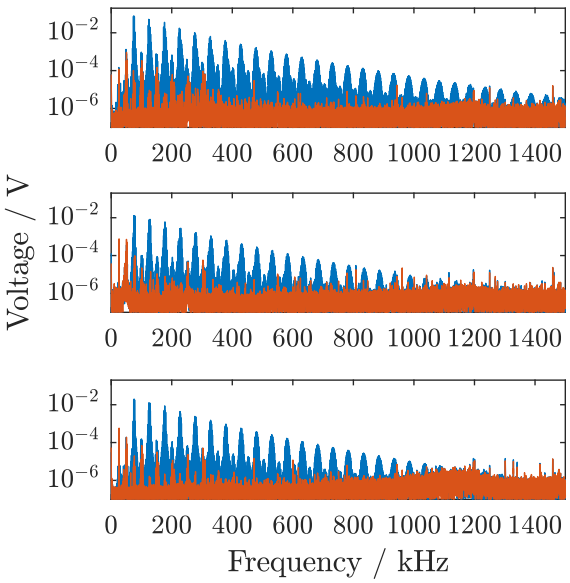

Figure 7: Measured results of three channels with 200 averages. The results of the receive signals with background subtraction are shown in blue, the remaining backgrounds are shown in red. Upper: channel X; Middle: channel Y; Lower: channel Z.

Cancellation Unit

Due to the coupling between the transmit coils and the receive coils, the induced signals also includes the excitation signals. The induced excitation signal is much stronger than the particle signal, therefore the particle signal cannot be resolved by the DAQ card. A band-stop filter (BSF) can be used to suppress the induced signals at the excitation frequency, but it also damps the particles signals, which can cause a loss of information. Another method is to cancel the excitation signals. The transmit and receive coil setups are built two times, while the receive coils are connected in series but with different polarity. In contrast to the generation unit, there is no sample placed in the cancellation unit. Thus, the direct feedthrough is canceled at full bandwidth while the particle signal remains unchanged [22].

Band-stop Filter

In practice, it is impossible to build identical setups and the phase difference of two coils cannot be adapted easily. Hence, a band-stop filter (BSF) is used to attenuate the coupling effect as well as the cross-coupling effect [23]. A more moderate attenuation factor is chosen, which ensures the lower harmonics of the induced signals are still in the dynamic range of the DAQ card.

Low-noise Amplifier

As the induced particle signals are very weak, a low-noise amplifier (LNA) is used to amplify the signals for matching the input range of the DAQ card without introducing further noise.

IV. Results and Discussion

The measurements have been performed using 30 µl of diluted Resovist with a concentration of 250 µmol (Fe)/l. The excitation magnetic field had a field strength of 12 mT/μ_0 in each spatial direction. The induced signals have been measured first without averaging the receive signal and second averaging 200 times. The corresponding measurement times are 21.6 ms and 4.3 s respectively. The empty measurements are recorded under same conditions with an empty sample chamber. In Figure 6 and Figure 7, the receive signals are shown after background subtraction for the channels X, Y, and Z. The remaining background signals are shown as a reference.

As it can be seen from Figure 6, harmonics up to 1 MHz in channel X and 0.8 MHz in channel Y and Z can be measured. In Figure 7 the signals with 200 averages are shown, harmonics up to 1.4 MHz in channel X and 1.1 MHz in channel Y and Z can be detected. As the receive coil of the channel X is shaped as a sand-clock and very close to the nanoparticles, it can detect higher harmonics than that in the channels Y and Z. As seen from the figures, the remaining background reference is

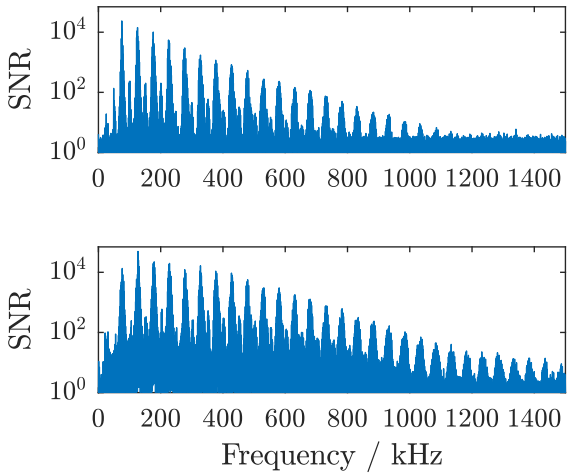

Figure 8: SNR results of X channel. Upper: without averaging; Lower: with 200 averages.

decreased due to the averaging.

In addition, the SNR at frequency k is calculated by

$$\mathrm{SNR}_k = \frac{\hat{u}_k}{\mathrm{std}(\hat{n}_k)},$$

where $\hat{u}_k$ is the spectral amplitude of the receive signals with background subtraction, $\mathrm{std}(\hat{n}_k)$ is the standard deviation of the remaining background. Here, the remaining background is measured 100 times to calculate the standard deviation. Figure 8 shows the SNR results of the X channel in the frequency domain. Without averaging, the largest SNR appears at the 3rd harmonic frequency, which is 2.4×10^4. In channel Y and Z, the largest SNR also at the 3rd harmonic frequency is 2.1×10^3 and 8.5×10^3, respectively. From Figure 8, after 200 averages the SNR results are much stronger. The largest SNR appears at the 5th harmonic, which is 4.9×10^4, 1.7×10^4 and 3.2×10^4 in channel X, Y and Z, respectively.

The sample used for measurement contains 418.84 µg iron. According to Rose model [24–26], a detection limit with a threshold SNR of 5 is assumed. Therefore, the detection limits are 87.26 ng without averaging and 42.74 ng with 200 averages. However, [27] suggests a procedure using a dilution series and the reconstructed data to determine the detection limit, which is more accurate and comparable.

V. Conclusion

In this paper, the first measurement results of a three-dimensional MPS are presented. Harmonics up to 1.1 MHz can be resolved in the measured signal, which exceeds the signal harmonics in the imaging systems and therefore can be used for image reconstruction. In addition, mixing-frequencies that are known to arise in multi-dimensional excitation can be seen. The number of detectable harmonics, as well as the presence of mixing frequencies, shows the suitability of the system to record three-dimensional hybrid system-matrices, as well as analysis of particle dynamics in three-dimensional space.

However, the system can be further improved. The low-noise amplifier used in the experiments are not specifically designed, an improvement for the detection limit of harmonics is possible and will be implemented. To record hybrid system-matrices, DC paths need to be added to every channel of the MPS. Subsequently, transmit and receive channel calibration have to be performed to quantify the measurement results [28].

Acknowledgment

This work was supported by the Federal Ministry of Education and Research, Germany (BMBF) under grant 13GW0069A.

References

[1] B. Gleich and J. Weizenecker. Tomographic imaging using the nonlinear response of magnetic particles. *Nature*, 435(7046):1214–1217, 2005, doi:10.1038/nature03808.

[2] J. Weizenecker, J. Borgert, and B. Gleich. A simulation study on the resolution and sensitivity of magnetic particle imaging. *Physics in Medicine and Biology*, 52(21):6363–6374, 2007, doi:10.1088/0031-9155/52/21/001.

[3] J. Weizenecker, B. Gleich, J. Rahmer, H. Dahnke, and J. Borgert. Three-dimensional real-time in vivo magnetic particle imaging. *Physics in Medicine and Biology*, 54(5):L1–L10, 2009, doi:10.1088/0031-9155/54/5/L01.

[4] J. Borgert, B. Gleich, J. Rahmer, H. Dahnke, and J. Weizenecker. Three-dimensional real-time in vivo magnetic particle imaging. *MedicaMundi*, 53(2):48–57, 2009.

[5] M. Gruettner, M. Graeser, S. Biederer, T. F. Sattel, H. Wojtczyk, W. Tenner, T. Knopp, B. Gleich, J. Borgert, and T. M. Buzug, 1D-image reconstruction for magnetic particle imaging using a hybrid system function, in *2011 IEEE Nuclear Science Symposium Conference Record*, 2545–2548, 2011. doi:10.1109/NSSMIC.2011.6152687.

[6] A. von Gladiss, M. Graeser, P. Szwargulski, T. Knopp, and T. M. Buzug. Hybrid system calibration for multidimensional magnetic particle imaging. *Physics in Medicine and Biology*, 62(9):3392–3406, 2017, doi:10.1088/1361-6560/aa5340.

[7] S. Biederer, T. Sattel, T. Knopp, K. Lüdtke-Buzug, B. Gleich, J. Weizenecker, J. Borgert, and T. M. Buzug, A Spectrometer for Magnetic Particle Imaging, in *4th European Conference of the International Federation for Medical and Biological Engineering*, 2009, 2313–2316. doi:10.1007/978-3-540-89208-3_555.

[8] S. Biederer, T. Knopp, T. F. Sattel, K. Lüdtke-Buzug, B. Gleich, J. Weizenecker, J. Borgert, T. M. Buzug, and K. Lüdtke-Buzug. Magnetization response spectroscopy of superparamagnetic nanoparticles for magnetic particle imaging. *Journal of Physics D: Applied Physics*, 42(20):205007, 2009, doi:10.1088/0022-3727/42/20/205007.

[9] S. Biederer, T. Knopp, T. F. Sattel, K. Lüdtke-Buzug, B. Gleich, J. Weizenecker, J. Borgert, and T. M. Buzug, Estimation of Magnetic Nanoparticle Diameter with a Magnetic Particle Spectrometer, in *World Congress on Medical Physics and Biomedical Engineering*, 2009, 61–64. doi:10.1007/978-3-642-03887-7_17.

[10] B. Gleich, J. Weizenecker, and J. Borgert. Experimental results on fast 2D-encoded magnetic particle imaging. *Physics in Medicine and Biology*, 53(6):N81–N84, 2008, doi:10.1088/0031-9155/53/6/N01.

[11] T. Knopp, J. Rahmer, T. F. Sattel, S. Biederer, J. Weizenecker, B. Gleich, J. Borgert, and T. M. Buzug. Weighted iterative reconstruction for magnetic particle imaging. *Physics in Medicine and Biology*, 55(6):1577–1589, 2010, doi:10.1088/0031-9155/55/6/003.

[12] T. Knopp, T. F. Sattel, S. Biederer, and T. M. Buzug, Limitations of measurement-based system functions in magnetic particle imaging, in *Medical Imaging 2010: Biomedical Applications in Molecular, Structural, and Functional Imaging*, 76261F, 2010. doi:10.1117/12.844181.

[13] T. Knopp, T. F. Sattel, S. Biederer, J. Rahmer, J. Weizenecker, B. Gleich, J. Borgert, and T. M. Buzug. Model-based reconstruction for magnetic particle imaging. *IEEE Transactions on Medical Imaging*, 29(1):12–18, 2010, doi:10.1109/TMI.2009.2021612.

[14] T. Knopp, S. Biederer, T. F. Sattel, J. Rahmer, J. Weizenecker, B. Gleich, J. Borgert, and T. M. Buzug. 2D model-based reconstruction for magnetic particle imaging. *Medical Physics*, 37(2):485–491, 2010, doi:10.1118/1.3271258.

[15] M. Graeser, S. Biederer, M. Grüttner, H. Wojtczyk, T. F. Sattel, W. Tenner, G. Bringout, and T. M. Buzug, Determination of System Functions for Magnetic Particle Imaging, in *Magnetic Particle Imaging: A Novel SPIO Nanoparticle Imaging Technique*, 2012, 59–64. doi:10.1007/978-3-642-24133-8_10.

[16] M. Graeser, A. von Gladiss, P. Szwargulski, M. Ahlborg, T. Knopp, and T. M. Buzug, Reconstruction of Experimental 2D MPI Data using a Hybrid System Matrix, in *International Workshop on Magnetic Particle Imaging*, 130, 2016.

[17] T. Wawrzik, J. Hahn, F. Ludwig, and M. Schilling, Magnetic particle spectrometry for the evaluation of field-dependent harmonics generation, in *Magnetic Nanoparticles: Particle Science, Imaging Technology, and Clinical Applications*, 86–90, 2010. doi:10.1142/9789814324687_0012.

[18] M. Graeser, M. Ahlborg, A. Behrends, K. Bente, G. Bringout, C. Debbeler, A. von Gladiss, K. Gräfe, C. Kaethner, S. Kaufmann, K. Lüdtke-Buzug, H. Medimagh, J. Stelzner, M. Weber, and T. M. Buzug, A device for measuring the trajectory dependent magnetic particle performance for MPI, in *International Workshop on Magnetic Particle Imaging*, 2015. doi:10.1109/IWMPI.2015.7107078.

[19] M. Graeser, A. von Gladiss, M. Weber, and T. M. Buzug. Two dimensional magnetic particle spectrometry. *Physics in Medicine and Biology*, 62(9):3378–3391, 2017, doi:10.1088/1361-6560/aa5bcd.

[20] X. Chen, A. Behrends, M. Graeser, A. Neumann, and T. M. Buzug, Optimizing the Coil Setup for a Three-Dimensional Magnetic Particle Spectrometer, in *International Workshop on Magnetic Particle Imaging*, 59, 2016.

[21] X. Chen, Implementation of the signal chains for a 3d magnetic particle imaging, unpublished Master Thesis, University of Luebeck, 2016,

[22] M. Graeser, T. Knopp, M. Grüttner, T. F. Sattel, and T. M. Buzug. Analog receive signal processing for magnetic particle imaging. *Medical physics*, 40(4):042303, 2013, doi:10.1118/1.4794482.

[23] M. Graeser, T. Knopp, T. F. Sattel, M. Gruettner, and T. M. Buzug, Signal separation in magnetic particle imaging, in *2012 IEEE Nuclear Science Symposium and Medical Imaging Conference Record*, 2483–2485, 2012. doi:10.1109/NSSMIC.2012.6551566.

[24] A. Rose. A Unified Approach to the Performance of Photographic Film, Television Pickup Tubes, and the Human Eye. *Journal of the Society of Motion Picture Engineers*, 47(4):273–294, 1946, doi:10.5594/J12772.

[25] A. Rose. The Sensitivity Performance of the Human Eye on an Absolute Scale. *Journal of the Optical Society of America*, 38(2):196, 1948, doi:10.1364/JOSA.38.000196.

[26] A. E. Burgess. The Rose model, revisited. *Journal of the Optical Society of America A*, 16(3):633, 1999, doi:10.1364/JOSAA.16.000633.

[27] M. Graeser, T. Knopp, P. Szwargulski, T. Friedrich, A. von Gladiss, M. Kaul, K. M. Krishnan, H. Ittrich, G. Adam, and T. M. Buzug. Towards Picogram Detection of Superparamagnetic Iron-Oxide Particles Using a Gradiometric Receive Coil. *Scientific Reports*, 7(1):6872, 2017, doi:10.1038/s41598-017-06992-5.

[28] S. Biederer, Entwicklung eines Spektrometers zur Analyse superparamagnetischer Eisenoxid-Nanopartikel für Magnetic-Particle-Imaging. Wiesbaden: Vieweg+Teubner Verlag, 2012, doi:10.1007/978-3-8348-2407-3.

